AJNR

MR and CT correlation of cholesterol cysts of the petrous bone.

C Griffin, R DeLaPaz and D Enzmann

AJNR Am J Neuroradiol 1987, 8 (5) 825-829
http://www.ajnr.org/content/8/5/825

MR and CT Correlation of Cholesterol Cysts of the Petrous Bone

Charles Griffin[1]
Robert DeLaPaz
Dieter Enzmann

Four patients with expansile cystic lesions of the petrous bone had correlative CT and MR scans. Characteristic findings were noted on MR scans obtained with T1- (TR = 400–800, TE = 25–32) and T2- (TR = 2000–3000, TE = 64–80) weighted images. These findings include an expansile cystic lesion centered in the petrous apex with high signal intensity on both the T1- and T2-weighted images, compatible with subacute or chronic hemorrhage. This signal pattern is distinct from the typical intradural epidermoid tumor, which has signal intensities similar to CSF with low signal on T1-weighted images and high signal on T2-weighted images. Surgical exploration yielded similar findings of a cyst containing free-flowing, brown watery fluid. Histologically, an inflammatory response was present as well as a variable number of cholesterol crystals. There was little identifiable capsular tissue but abundant evidence of subacute or chronic hematoma.

The nomenclature of the etiology in these four cases is currently in some controversy, with some authors classifying these lesions as epidermoid or primary cholesteatomas while others call them cholesterol granulomas or giant cholesterol cysts. Whatever they are named, the MR image pattern is consistent and is dominated by findings indicative of hemoglobin breakdown products.

Expansile cystic lesions of the petrous apex and petrous bone have been thought to be secondary to epidermoids (primary cholesteatomas) and giant cholesterol cysts, sometimes called cholesterol granulomas [1–3]. Criteria have been described [3] for the differentiation of these entities but in practice the pathologic findings may not allow clear differentiation. This report describes the CT and MR characteristics of these lesions and correlates these with the surgical findings. Emphasis is placed on the constant surgical finding of a hemorrhagic cyst that can be predicted preoperatively by MR criteria.

Subjects and Methods

MR imaging was performed in four patients, two females and two males, ranging in age from 16 to 47 years old. The clinical presentation was variable, from increasingly severe headaches ipsilateral to the lesion to progressive 7th and 8th nerve dysfunction (see Table 1). In three patients MR imaging was performed on a 1.5-T scanner (GE Signa) using T1-weighted (TR = 400–800 msec, TE = 20–25 msec) and T2-weighted (TR = 2000 msec, with asymmetrical TE = 20–25 and 80 msec) sequences acquired with a multislice, multiecho, spin-echo technique and a 256 × 256 matrix. One patient was imaged at an outside institution with a Diasonics unit operating at 0.35 T using a T1-weighted sequence (TR = 732 msec, TE = 32 msec) and a T2-weighted sequence (TR = 3000 msec, TE = 64 msec). T1-weighted sequences were used for sagittal, axial, and coronal views; T2-weighted scans were obtained in an axial projection. All patients had recent high-resolution CT with IV contrast and underwent surgical exploration of their temporal bone lesions.

Results

High-resolution CT revealed similar findings in all four patients. Expansile lesions were centered in the petrous portion of the temporal bone (Fig. 1). In three lesions

Received December 30, 1986; accepted after revision April 1, 1987.

[1] All authors: Department of Radiology, Stanford University School of Medicine, Stanford, CA 94305. Address reprint requests to D. Enzmann.

AJNR 8:825–829, September/October 1987
0195–6108/87/0805-0825

TABLE 1: Clinical Data Summary

Age	Gender	Symptoms	CT		MR		Disease
			+	−	T1-Weighted Image	T2-Weighted Image	
16	F	Severe unilateral headaches	=	=	++	++	Chronic hemorrhage, inflammatory infiltrate, cholesterol clefts
24	M	7th and 8th nerve dysfunction	=	=	++	++	Chronic hemorrhage, inflammatory infiltrate
27	F	7th and 8th nerve dysfunction	=	=	++	++	No microscopic cyst containing old blood
47	M	7th and 8th nerve dysfunction	=	=	++	++	No microscopic cyst containing old blood

Note.—++, significantly higher signal intensity or attenuation than surrounding brainstem parenchyma; =, signal intensity or attenuation equal to surrounding brainstem parenchyma.

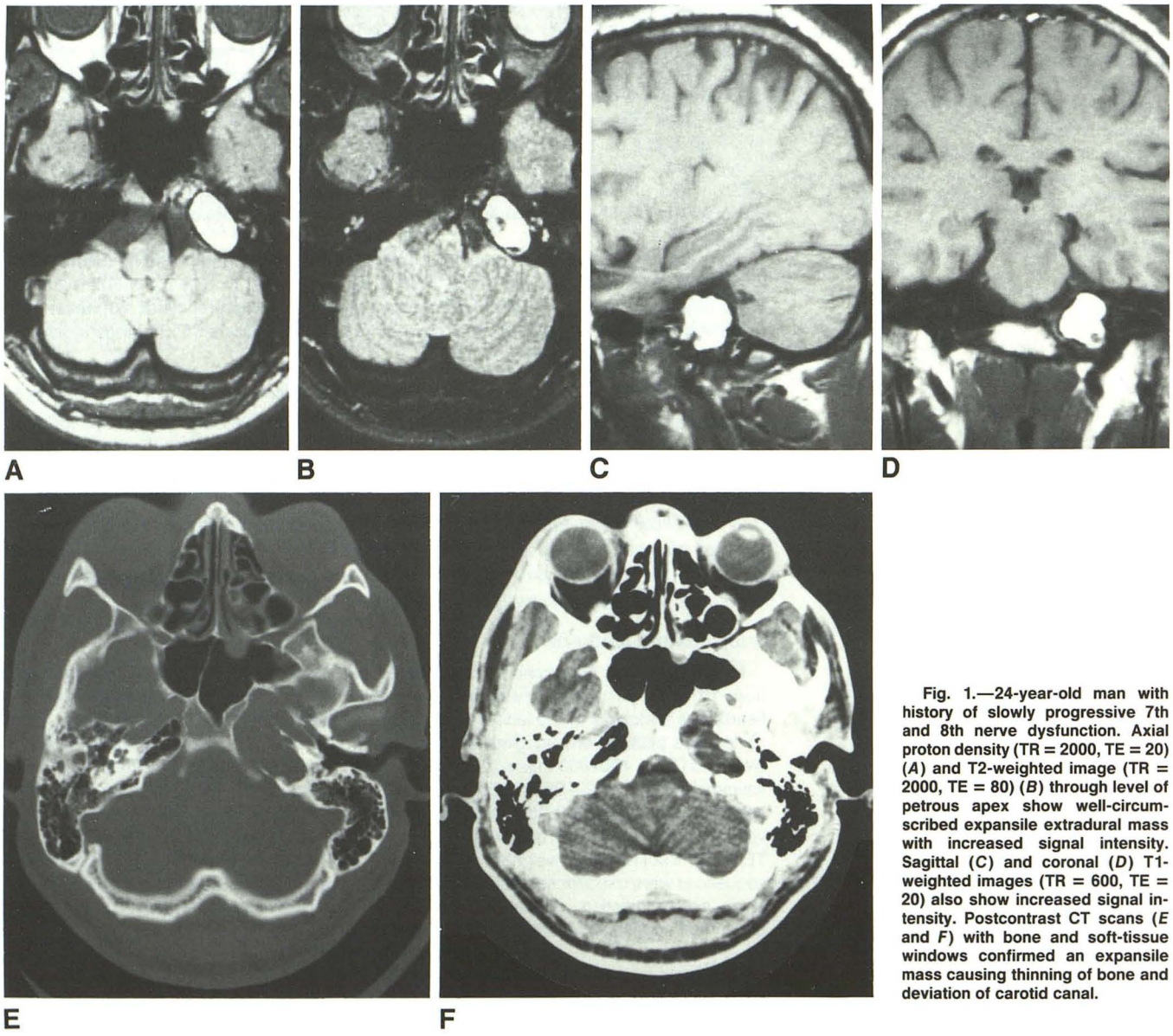

Fig. 1.—24-year-old man with history of slowly progressive 7th and 8th nerve dysfunction. Axial proton density (TR = 2000, TE = 20) (*A*) and T2-weighted image (TR = 2000, TE = 80) (*B*) through level of petrous apex show well-circumscribed expansile extradural mass with increased signal intensity. Sagittal (*C*) and coronal (*D*) T1-weighted images (TR = 600, TE = 20) also show increased signal intensity. Postcontrast CT scans (*E* and *F*) with bone and soft-tissue windows confirmed an expansile mass causing thinning of bone and deviation of carotid canal.

the epicenter was the petrous apex. One large lesion completely surrounded the cochlea and vestibular apparatus (Fig. 2D). These lesions had attenuation values of soft tissue or slightly lower and none showed central contrast enhancement. One case showed peripheral enhancement adjacent to the overlying dura. The larger, more expansile lesions had a very thin rim of bone but in some areas no bone margin could be seen.

All the lesions seen on CT were identified on MR. The MR findings were consistent in all four patients. Each had increased signal intensity on both the T1- and the T2-weighted images (Figs. 1A, 1B, 2A, and 2C). The increased signal intensity was homogeneous except for a variable number of thin, low-signal-intensity bands or "septations" running through the central portions of the cysts in all patients. In one patient a portion of the cyst extended into the internal auditory canal (Figs. 2A, 2B, and 2C). One patient had a lesion with identical MR signal characteristics in the opposite petrous apex and only minimal expansion.

In all patients surgery revealed a free-flowing, brown cystic fluid. In two patients no preparations were made to collect the fluid and because of its free-flowing nature adequate quantities for pathologic inspection could not be obtained. In the remaining two patients the fluid revealed multiple hemosiderin-laden macrophages with a positive iron stain, multinucleated giant cells, and amorphous debris consistent with keratin. Fluid analysis in one of these two patients revealed total bilirubin of 6.9 mg/dl (normal for blood = 0.2–1.0), total protein of 8.0 g/dl (normal for blood = 6–8 g/dl), cholesterol 295 mg/dl (normal for blood = 100–260), and triglycerides of 85 mg/dl (normal for blood = 35–160). In no lesion could a well-defined cyst wall be identified. In two patients very small pieces of what was thought to represent cyst wall were examined. One revealed only bland cuboidal epithelium thought to be inner ear epithelium. It also showed organizing granulation tissue with focally prominent lymphohistiocytic inflammatory infiltrate, foci of subacute and chronic hemorrhage, cholesterol ester clefts with giant cell reaction, and some acellular eosinophilic material that was suggestive of keratinous squamae (Figs. 3A and 3B). The second showed a hyalinized fibrous lining with an adjacent layer of inflammatory cells. This specimen was very poorly cellular and showed

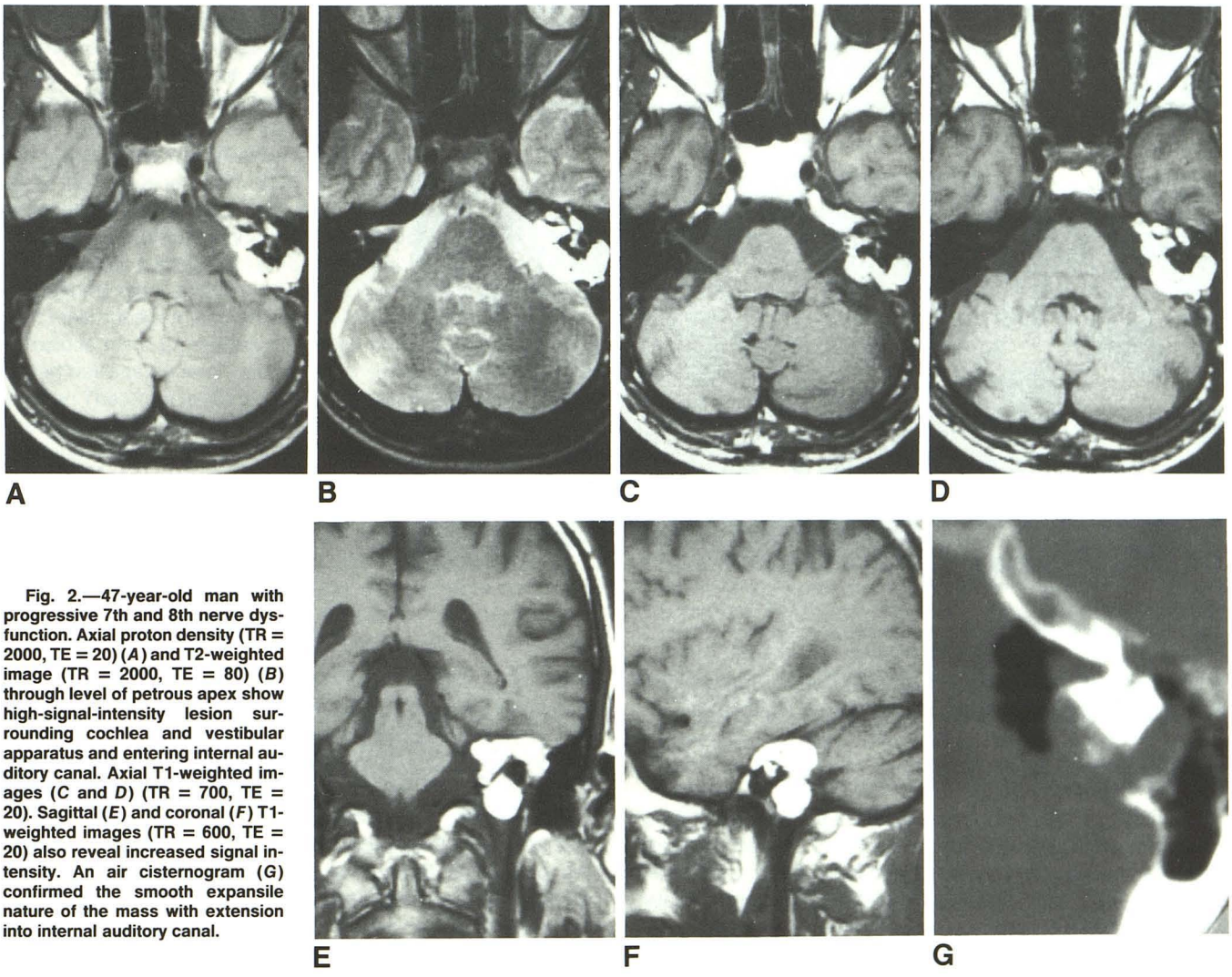

Fig. 2.—47-year-old man with progressive 7th and 8th nerve dysfunction. Axial proton density (TR = 2000, TE = 20) (*A*) and T2-weighted image (TR = 2000, TE = 80) (*B*) through level of petrous apex show high-signal-intensity lesion surrounding cochlea and vestibular apparatus and entering internal auditory canal. Axial T1-weighted images (*C* and *D*) (TR = 700, TE = 20). Sagittal (*E*) and coronal (*F*) T1-weighted images (TR = 600, TE = 20) also reveal increased signal intensity. An air cisternogram (*G*) confirmed the smooth expansile nature of the mass with extension into internal auditory canal.

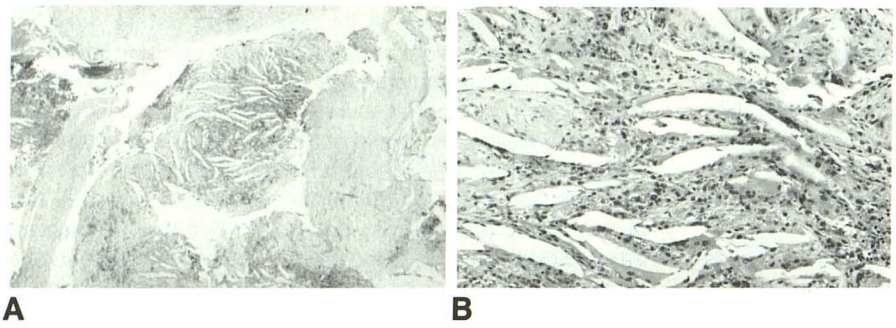

Fig. 3.—24-year-old man with history of slowly progressive 7th and 8th nerve dysfunction. Low- (25×) (*A*) and high- (125×) (*B*) power photomicrographs show multiple fragments of organizing granulation tissue of varying maturity with focally prominent lymphohistocytic inflammatory infiltrate and scattered foci of acute and chronic hemorrhage. Numerous cholesterol ester clefts are distributed throughout granulation tissue with exuberant giant cell reaction.

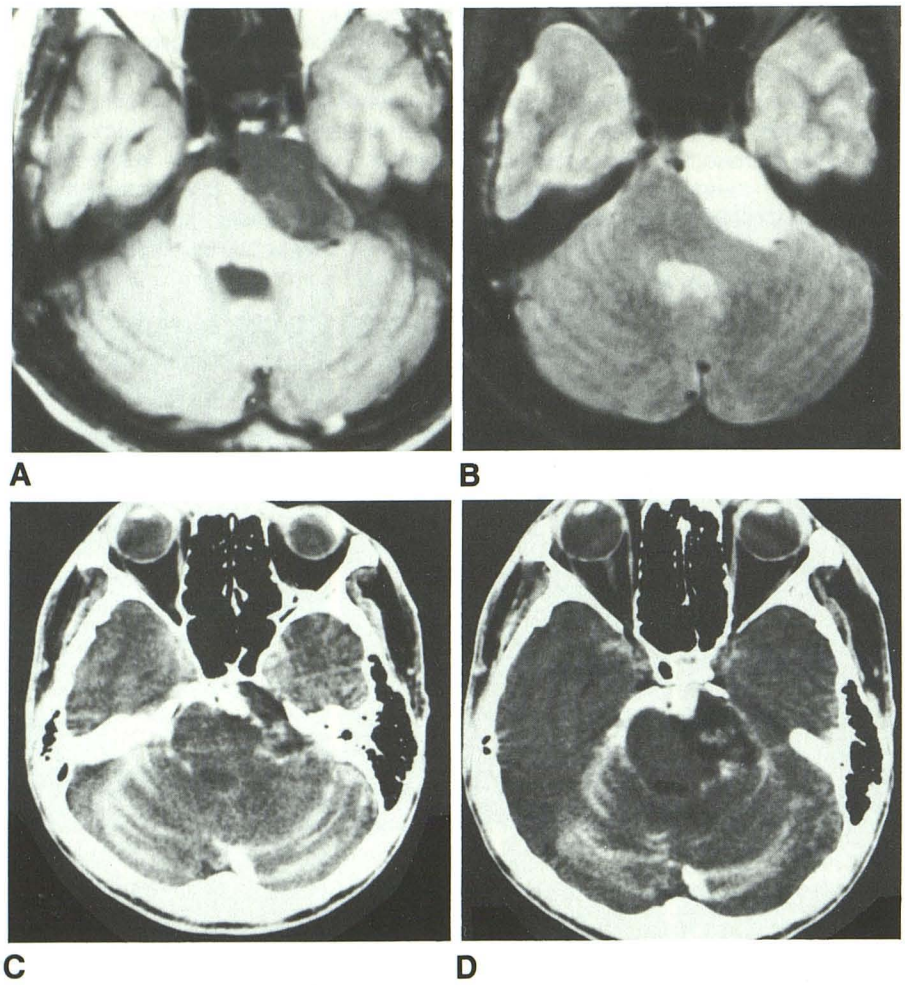

Fig. 4.—29-year-old asymptomatic man evaluated with CT before heart transplant. T1- (TR = 400, TE = 25) (*A*) and T2- (TR = 2000, TE = 80) (*B*) weighted images show left cerebellopontine angle intradural extraaxial mass with internal signal inhomogeneity most prominent on T1-weighted image. CT scans (*C* and *D*) with intrathecal metrizamide and with *C* at same level as *A* show contrast entering interstices of the mass compatible with a diagnosis of epidermoid tumor. Note difference from petrous apex cystic lesions, especially on T1-weighted image.

only occasional multinucleated giant cells and numerous lymphocytes, plasma cells, and a few scattered eosinophils.

Discussion

The pathology of petrous apex cystic lesions is under some controversy. Two lesions that are said to be pathologically distinct appear to share many pathologic criteria, are often confused, and many times are interchanged diagnostically. One lesion is called primary cholesteatoma (also called epidermoid cholesteatoma) and the other is cholesterol granuloma (also called cholesterol cyst) [4–12]. A recent paper reviewing the literature distinguished these two entities [3]. The authors described the cholesterol granuloma as containing brown semiliquid material composed of multinucleated foreign-body-type giant cells, cholesterol in the acicular clefts, blood vessels, fibrous tissue, red blood cells, hemosiderin, and chronic inflammatory cells. This corresponds closely to the pathologic findings in this series of patients. Primary cholesteatoma on the other hand appeared pearly white with friable material composed of squamous epithelium with desquamated keratin. However, several authors [13–16] men-

tion intracranial epidermoids that had high attenuation on noncontrast scans and describe their contents as a mixture of debris and blood within walls containing hemosiderin, hemosiderin-laden macrophages, giant cells, and clefts of cholesterol crystals—descriptions strikingly similar to those of cholesterol granulomas [3]. The authors also describe these two entities as frequently coexisting.

It seems unlikely that all these lesions are initiated by a true congenital rest of epidermal cells. Previous studies of 124 temporal bones by Ruedi [17] revealed no evidence of congenital epithelial rests. It is thought that a significant number of these lesions are initiated by chronic obstruction to the ventilation and drainage of pneumatized spaces [7, 9]. This results in mucosal edema and multiple hemorrhages with formation of cholesterol crystals that cause a sterile inflammatory response and giant-cell formation. It appears as if an important common denominator for the continued evolution of these lesions independent of the initiating cause is multiple hemorrhages. The lesions we have described may be the result of a final common pathway for the various pathologic entities described above. These hemorrhages cause a characteristic appearance on MR; increased signal on both T1- and T2-weighted images secondary to the paramagnetic effect of heme iron (Fe 3+) in methemoglobin or other hemoglobin breakdown products, combined with a high proton density. This MR appearance is quite different from intradural epidermoid tumors, which reveal low signal on T1-weighted images and high signal on T2-weighted images closely paralleling the signal intensities of CSF (Figs. 4A and 4B). They can be distinguished from CSF by significant internal signal inhomogeneity caused by their internal structure [18–20].

The thin rim of low signal intensity characteristically seen in parenchyma surrounding chronic hematomas secondary to the magnetic susceptibility effects of ferritin in hemosiderin-laden macrophages was not seen in these patients [21]. All the lesions were extradural and were covered by either expanded petrous bone or dura, both of which have low signal intensity. Therefore, even if sufficient amounts of hemosiderin were present to produce a magnetic susceptibility effect it would be difficult to detect. In those areas in which the hemorrhagic contents of these lesions abutted brain parenchyma this susceptibility effect was also not visualized. One patient had a lesion with identical MR signal characteristics in the opposite petrous apex. CT revealed only minimal expansion. This lesion was asymptomatic and therefore not surgically explored. Presumably it is the same disease process as the contralateral petrous apex but at an earlier or arrested stage of development. Lesions with these findings have been identified in asymptomatic patients. We have recommended a conservative course of periodic (1–2 yr) reimaging to monitor evolution in the size of the lesions. If these lesions progress they probably do so very slowly. Occasionally, a nonaerated petrous apex with prominant medullary fat can be mistaken for a nonexpansile hemorrhagic petrous apex lesion on the T1-weighted image. These can always be distinguished on MR with a T2-weighted sequence showing lower signal paralleling other medullary fat. CT can also be helpful in showing attenuation compatible with medullary bone. Most neoplastic mass lesions of the petrous bone are not hemorrhagic and can be distinguished from the lesions described here by the presence of low signal on T1-weighted images and high signal on T2-weighted images.

In conclusion, regardless of the name used for these expansile cystic lesions, their MR characteristics are consistent and predictive of the surgical findings. The MR characteristics allow differentiation from intradural epidermoids and nonhemorrhagic neoplastic mass lesions whereas CT may not.

REFERENCES

1. Latack JT, Kartush JM, Kemink JL, Graham MD, Knake JE. Epidermoidomas of the cerebellopontine angle and temporal bone: CT and MR aspects. *Radiology* **1985**;157:361–366
2. Latack JT, Graham MD, Kemink JL, Knake JE. Giant cholesterol cysts of the petrous apex: radiologic features. *AJNR* **1985**;6:409–413
3. Lo WWM, Solti-Bohman LG, Brackmann DE, Gruskin P. Cholesterol granuloma of the petrous apex: CT diagnosis. *Radiology* **1984**;153:705–711
4. Friedman I. Epidermoid cholesteatoma and cholesterol granuloma. *Ann Otol Rhinol and Laryngol* **1959**;68:57–79
5. Sheehy JL, Linthicum FH Jr, Greenfield EC. Chronic serous mastoiditis, idiopathic hemotympanum and cholesterol granuloma of the mastoid. *Laryngoscope* **1969**;79:1189–1217
6. Yanagihara N, Matsumoto Y. Cholesteatoma in the petrous apex. *Laryngoscope* **1981**;91:272–278
7. Plester D, Steinbach E. Cholesterol granuloma. *Otolaryngol Clin North Am* **1982**;15:665–672
8. Gacek RR. Evaluation and management of primary petrous apex cholesteatoma. *Otolaryngol Head Neck Surg* **1980**;88:519–523
9. Nager GT, Vanderveen TS. Cholesterol granuloma involving the temporal bone. *Ann Otol Rhinol Laryngol* **1976**;85:204–209
10. Friedmann I, Graham MD. The ultrastructure of cholesterol granuloma of the middle ear. *J Laryngol Otol* **1979**;93:433–442
11. House JL, Brackmann DE. Cholesterol granuloma of the cerebellopontine angle. *Arch Otolaryngol* **1982**;108:504–506
12. Wyler AR, Leech RW, Reynolds AF, Ojeman GA, Mead C. Cholesterol granuloma of the petrous apex. *J Neurosurg* **1974**;41:765–768
13. Schubiger O, Valavanis A, Gessaga E. Dense suprasellar epidermoid cyst. A case report. *Neuroradiology* **1983**;24:269–271
14. Braun IF, Nadich TP, Leeds NE, Koslow M, Zimmerman HM, Chase NE. Dense intracranial epidermoid tumors. *Radiology* **1977**;122:717–719
15. Hasegawa H, Bitoh S, Nakata M, Fufiwara M, Yasuda H. Intracranial epidermoid mimicking meningioma *Surg Neurol* **1981**;15:372–374
16. Dunn RC Jr, Archer CA, Rapport RL, Looi LM. Unusual CT-dense posterior fossa epidermoid cyst. Case report. *J Neurosurg* **1981**;55:654–656
17. Ruedi I. Cholesteatosis of the attic. *J Laryngol* **1958**;72:593
18. Kortman KE, Bradley WG. Magnetic resonance imaging of epidermoid tumors. Presented at the annual meeting of the Western Neuroradiological Society, Monterey, CA, October **1985**
19. Berger M, Wilson C. Epidermoid cysts of the posterior fossa. *J Neurosurg* **1985**;62:214–219
20. Davidson HD, Ouchi T, Steiner RE. NMR imaging of congenital intracranial germinal layer neoplasms. *Neuroradiology* **1985**;27:301–303
21. Gomori JM, Grossman RI, Goldberg HI, Hackney DB, Zimmerman RA, Bilaniuk LT. Intracranial hematomas: imaging by high-field MR. *Radiology* **1985**;157:87–93